Cellular Signalling 48 (2018) 13–24

Contents lists available at ScienceDirect

Cellular Signalling

journal homepage: www.elsevier.com/locate/cellsig

S6 kinase 1 plays a key role in mitochondrial morphology and cellular energy flow

Quangdon Tran[a], Jae-Hun Jung[b], Jisoo Park[a], Hyunji Lee[a], Youngeun Hong[a], Hyeonjeong Cho[a], Minhee Kim[a], Sungjin Park[a], So-Hee Kwon[d], Seon-Hwan Kim[e], George Thomas[f], Kwang Pyo Kim[b,c,*], Myung-Haing Cho[g,**], Jongsun Park[a,**]

[a] Department of Pharmacology and Medical Science, Metabolic Syndrome and Cell Signaling Laboratory, Institute for Cancer Research, College of Medicine, Chungnam National University, Daejeon 35015, South Korea
[b] Department of Applied Chemistry, Institute of Natural Science, Global Center for Pharmaceutical Ingredient Materials, Kyung Hee University, Yongin 17104, South Korea
[c] Department of Biomedical Science and Technology, Kyung Hee Medical Science Research Institute, Kyung Hee University, Seoul 02447, Republic of Korea
[d] College of Pharmacy, Yonsei Institute of Pharmaceutical Sciences, Yonsei University, Incheon 21983, South Korea
[e] Department of Neurosurgery, Institute for Cancer Research, College of Medicine, Chungnam National University, Daejeon 35015, South Korea
[f] Laboratory of Metabolism and Cancer, Catalan Institute of Oncology, ICO, Bellvitge Biomedical Research Institute, IDIBELL, 08908 Barcelona, Spain
[g] Laboratory of Toxicology, College of Veterinary Medicine Seoul National University, Seoul 08826, South Korea

ARTICLE INFO

Keywords:
S6K1
Drp1
Fission
Metabolic shift
Mitophagy
OxPhos

ABSTRACT

Mitochondrial morphology, which is associated with changes in metabolism, cell cycle, cell development and cell death, is tightly regulated by the balance between fusion and fission. In this study, we found that S6 kinase 1 (S6K1) contributes to mitochondrial dynamics, homeostasis and function. Mouse embryo fibroblasts lacking S6K1 (S6K1-KO MEFs) exhibited more fragmented mitochondria and a higher level of Dynamin related protein 1 (Drp1) and active Drp1 (pS616) in both whole cell extracts and mitochondrial fraction. In addition, there was no evidence for autophagy and mitophagy induction in S6K1 depleted cells. Glycolysis and mitochondrial respiratory activity was higher in S6K1-KO MEFs, whereas OxPhos ATP production was not altered. However, inhibition of Drp1 by Mdivi1 (Drp1 inhibitor) resulted in higher OxPhos ATP production and lower mitochondrial membrane potential. Taken together the depletion of S6K1 increased Drp1-mediated fission, leading to the enhancement of glycolysis. The fission form of mitochondria resulted in lower yield for OxPhos ATP production as well as in higher mitochondrial membrane potential. Thus, these results have suggested a potential role of S6K1 in energy metabolism by modulating mitochondrial respiratory capacity and mitochondrial morphology.

1. Introduction

Mitochondria are critical cellular organelles, best known for their role in providing efficient energy support through the chemiosmotic process of oxidative phosphorylation (OxPhos). In the 1960s, their role in aerobic energy transduction through the characteristic chemiosmotic mechanism of OxPhos first began to be clarified [1,2]. Since then, mitochondria have also been shown to perform a variety of roles in processes such as the transduction of metabolic and stress signals [2–5], the production of free radicals such as reactive oxygen species (ROS) [4,6], and the induction of programmed cell death [2,5,7]. The accumulation of damaged mitochondria can be unfavorable to cells. Mitochondrial quality and quantity are therefore strictly monitored to ensure balanced cell physiology. Damaged or unwanted mitochondria can be selectively removed by mitochondrial autophagy or mitophagy, a catabolic process for lysosome-dependent degradation. The molecular mechanism of mitophagy has begun to emerge. Several mitophagy receptors have been reported, including: ATG32 in yeast [8,9], NIX/BNIP3L [10], BNIP3 [11], fun14 domain-containing protein 1 (FUNDC1) in mammalian cells [12] interacting with LC3 via their conserved LC3 interaction region for mitophagy. E3 ubiquitin ligase Parkin and phosphatase and tensin homolog (PTEN)-induced putative protein kinase 1 (PINK1) also have critical functions for the removal of depolarized mitochondria [13,14].

* Correspondence to: Kwang Pyo Kim, Department of Applied Chemistry, Institute of Natural Science, Global Center for Pharmaceutical Ingredient Materials, Kyung Hee University, Yongin, 17104
** Corresponding authors.
E-mail addresses: kimkp@khu.ac.kr (K.P. Kim), mchotox@snu.ac.kr (M.-H. Cho), insulin@cnu.ac.kr (J. Park).

https://doi.org/10.1016/j.cellsig.2018.04.002
Received 16 January 2018; Received in revised form 5 April 2018; Accepted 13 April 2018
Available online 17 April 2018

Mitochondrial functional flexibility is matched by their morphological and structural change. During the lifetime of a cell, the mitochondrial network is continuously shaped by fission and fusion events [15]. Proteins involved in both the regulation and maintenance of mitochondrial morphology have crucial roles in maintaining the health of the cell [16,17]. The dynamin-related GTPases optic atrophy 1 (OPA1) of the inner mitochondrial membrane [18], and mitofusins (MFN) 1 and 2 of the outer membrane [19] regulate mitochondrial fusion in mammalian cells. Reversely, the master regulator of mitochondrial fission is a cytosolic member of the dynamin family of GTPases termed Drp1 (Dynamin-related protein 1). Drp1 polymerises around mitochondria, and through GTP hydrolysis constricts the mitochondria leading to membrane scission [20,21]. Drp1 activity at the mitochondrial outer membrane is regulated by not only interactions with mitochondrial accessory and effector proteins such as MFF, Fis1 [24] but also by post-translational such as phosphorylation [23,24].

Ribosomal S6 kinase 1 (S6K1), a member of the AGC family of serine/threonine protein kinases [25,26] has been linked to diverse cellular processes, including protein synthesis, mRNA processing, glucose homeostasis, cell growth and survival. S6K1 activity plays in a number of pathologies, including obesity, diabetes, ageing and cancer [27]. In 2004, Um et al. showed that S6K1 depletion increased UCP expression and resulted in protecting mice from diet-induced obesity [28]. However, as part of that protective phenotype, the morphology as well as the activity of mitochondria, which tightly link nutrient utilization and energy expenditure [29], were not elucidated. In this report, we demonstrated that the depletion of S6K1 induced mitochondrial fission but not mitophagy. These changes in mitochondrial morphology alter the function of mitochondria, disrupting the balance of OxPhos ATP production and shifting cellular energy metabolism. These data provide new insights into the role of S6K1 in mitochondrial biology and cellular energy regulation.

2. Materials and methods

2.1. Antibodies and reagents

Anti-Drp1 (#611112), anti-Rip1 (#610459) and anti-Opa1 (#612606) antibody were purchased from BD Biosciences (San Jones, USA). Anti-LC3B (#L7543), anti-Actin (#A5316) anti-Fis1 (#PA5-22142) antibodies were from Sigma-Aldrich (St. Louis, USA), anti-pDrp1 (pS616 (#3455S) or pS637 (#58675)) were purchased from Cell Signaling Technology (Boston, USA), anti-Tom40 (#SC-11414), and anti-S6K1 (#SC230) were obtained from Santa Cruz Biotechnology (Texas, USA). Anti-normal IGG (#L7543) and Horseradish peroxidase-conjugated anti-mouse IgG (#K0211589) or anti-rabbit IgG (#K0211708) secondary antibodies were from Komabiotech (Seoul, Korea). Alexa flour 488 anti-rabit antibody was purchased from Invitrogen (Oregon, USA). Anti-MFN2 (#ab56889) was from Abcam (Cambridge, United Kingdom). Carbonyl cyanide 3-chlorophenylhydrazone (CCCP), 2-deoxy-D-glucose (2DG), dichloroacetic acid (DCA), oligomycin and other chemicals for OxPhos activity assay were purchased from Sigma-Aldrich (St. Louis, USA). ATP assay kit was purchased from Invitrogen (Oregon, USA).

2.2. Cell culture and stimulation

S6K1-WT MEFs and S6K1-KO MEFs were maintained in medium (DMEM) supplemented with 10% FBS, 1% Antibiotics-Antimycotics (Heathcare life sciences, Utah, USA). These cells were transfected using Lipofectamine (Invitrogen, Oregon, USA) and jet-PEI (Polyplus, New York, USA) reagents following the instructions provided by manufacturers. Cells were treated with 30 μM CCCP for 8 h, 25 mM 2DG for 3 h, 30 mM DCA for 3 h and 2 μM oligomycin for 3 h before the ATP measurement.

2.3. Immunoblot analysis

The western blot analysis was performed as the described previously [30,31]. After the completion of experimental conditions, cells were placed on ice and extracted with lysis buffer containing 50 mM Tris-HCl, pH 7.5, 1% v/v Nonidet P-40, 120 mM NaCl, 25 mM sodium fluoride, 40 mM β-glycerol phosphate, 0.1 mM sodium orthovanadate, 1 mM phenylmethylsulfonyl fluoride (PMSF), 1 mM benzamidine, and 2 μM microcystin-LR. Lysates were centrifuged for 15 min at 12,000 *g*. The cell extracts were resolved by 15, 12 and 10% SDS-PAGE, and transferred to Immobilon-P membranes (Millipore, Darmstadt, Germany). The filters were blocked for 1 h in 1 × tri-buffered saline buffer (TBS; 140 mM NaCl, 2.7 mM KCl, 250 mM Tris-HCl, pH 7.4), containing 5% skimmed milk and 0.2% Tween-20, followed by an overnight incubation with the primary antibodies diluted 1000 folds at 4 °C. The secondary antibody was horseradish peroxidase-conjugated anti-mouse IgG or anti-rabbit IgG (Komabiotech, Seoul, Korea), diluted 5000-fold in the blocking buffer. The detection of protein expression was visualized by enhanced chemiluminescence, according to the manufacturer's instructions (Healthcare life sciences, Utah, USA).

2.4. Confocal imaging analysis

Cells were grown on glass coverslips until they were 50–70% confluent and then transfected with pDsRed2-Mito, GFP-Parkin-WT or GFP-LC3B constructs by using jet PEI reagents. After 48 h, the cells were fixed in 4% paraformaldehyde and permeabilized in 0.2% Triton-× 100 for 5 min at room temperature. Then the coverslips were mounted with Vectashield mounting solution (Vector Laboratories, Burlingame, USA), and visualized using a Zeiss confocal microscope. For immune fluorescence staining, after fixation and permeabilization, cells were block with 3%BSA in PBS for 2 h at room temperature followed by an overnight incubation with the primary antibodies (p616-Drp1) diluted 100 folds at 4 °C. The secondary antibody was, Alexa flour 488 anti-rabbit antibody, diluted 100-fold in the blocking buffer. Then the coverslips were mounted with Vectashield mounting solution (Vector Laboratories, Burlingame, USA), and visualized using confocal microscope.

2.5. Immunoprecipitation

HEK293 cells were transfected with pCDNA3.1 Empty vector or pCDNA3.1-Myc-S6K1 for 24 h, then placed on ice and extracted with lysis buffer containing 50 mM of Tris-HCl (pH 7.5), 0.5% v/v Nonidet P-40, 250 mM of NaCl, 3 mM of EDTA (pH 8.0), 3 mM of EGTA (pH 8.0), 40 mM of h-glycerol phosphate, 0.1 mmol/L of sodium orthovanadate, 1 mmol/L of phenylmethylsulfonyl fluoride, 1 mmol/L of benzamidine, and 2 μmol/L of microcystin-LR. S6K1 protein was immunoprecipitated from 1000 μg of cell-free extracts with normal IgG or anti-S6K1 antibody. The immune complexes were washed three times separated on SDS-PAGE and processed immunoblotting with anti-Rip1 antibody.

2.6. Flow cytometry (FACS) analysis for mitochondrial membrane potential and mass

S6K1-WT MEFs and S6K1-KO MEFs were plated for 24 h. Then cells were collected by trypsinization and stained with mito-green, JC-1 (Molecular probes, Invitrogen) for 30 min in turn in order to measure mitochondrial mass and mitochondrial membrane potential. The cells then were washed and analyzed with mission filters by BD FACS Canto system (BD Biosciences, San Jones, USA). For mito-green tracker: FITC value represent for mitochondrial mass. For JC-1 set: the cells were analyzed using 488 nm excitation with 530/30 nm and 585/42 nm bandpass emission filters; JC-1 can selectively enter into mitochondria and reversibly change color from red to green as the membrane potential decreases. With high mitochondrial ΔΨm, JC-1 spontaneously

forms J-aggregates exploring intense red fluorescence. With low ΔΨm, JC-1 remains in the monomeric form, which shows only green fluorescence. The mitochondrial membrane potential is represented as a ratio of PE/FITC value. Cells were treated with 30 μM CCCP for 10 min as a positive control to induce mitochondrial depolarization before staining with the dye.

2.7. Transmission electron microscopy

S6K1-WT MEFs and S6K1-KO MEFs were fixed in a solution of 2.5% glutaraldehyde with 1% osmium oxide (OsO_4) buffer for 1 h at 4 °C, dehydrated with ethanol at 4 °C. Then cells were infiltrated in a 1:1 mixture of propylene oxide and Epon and finally embedded in Epon by polymerization at 60 °C for 48 h. Ultrastructural analyses were performed on a SPIRIT G2 electron microscope.

2.8. Measurement of lactate in the culture medium

S6K1-WT MEFs and S6K1-KO MEFs were plated in 6-well plate, then after 24 h cultured media were harvested and filtered through a 10 kDa cut-off spin filter for lactate sample. The assays were measured according to the manufacturer's instructions (lactate assay kit, Sigma-Aldrich, Louis, USA).

2.9. Isolation of mitochondria and mitochondrial proteomic analysis

Cells were washed with PBS and suspended in mitochondrial fractionation buffer (20 mM Hepes, pH 8.0, 10 mM KCl, 1.5 mM MgCl2, 1 mM EDTA, 250 mM sucrose, 1 mM PMSF, 10 g/ml leupeptin, 10 g/ml aprotinin, and 0.2 mM sodium orthovanadate) for 15 min on ice and then homogenized using 1 ml syringe. Unbroken cells and nuclei were pelleted by centrifugation at 800 *g* for 10 min at 4 °C. The supernatant was continuously centrifuged at 17,000 *g* for 10 min at 4 °C and the supernatant was transferred to a new tube to be used as a cytosolic fraction. The pellet was washed with 500 μl of mitochondrial fractionation buffer, and used as isolated mitochondrial fraction. The mitochondrial fraction was analyzed by western blotting or OxPhos activity assay. At the same time, mitochondrial fraction was used for proteomic analysis.

2.10. Preparation of mitochondrial sample for proteomic analysis

Mitochondria protein digestion were performed by filter-aided sample preparation method [32]. Briefly, protein samples (100 μg) were reduced by adding SDT lysis buffer (4% sodium dodecyl sulfate (SDS) and 0.1 M dithiothreitol in 0.1 M Tris-HCl, pH 7.6) and transferred to the filtration devices (Microcon devices, YM-30, Millipore, MA). SDS from the proteins was washed with urea solution (0.2 ml of 8 M urea in 0.1 M Tris–HCl, pH 8.5) using centrifugation, followed by alkylation with 50 mM iodoacetamide in urea buffer solution. Filters were washed three times with ureic acid buffer followed by washes with 40 mM NH_4HCO_3. Protein digestion was conducted overnight with trypsin. After the first digestion, the second digestion was performed using trypsin for 6 h [33]. The eluted tryptic peptides were fractionated by isoelectrofocusing (IEF) fractionation, the 3100 OFFGEL fractionator with a "Low Resolution Kit" pH 3–10 (Agilent Technologies, Santa Clara, USA) according to the manufacturer's instructions.

2.11. Protein identification by liquid chromatography tandem-mass spectrometry (LC-MS/MS)

The desalted and fractionated peptides were analyzed using the Q-Exactive orbitrap hybrid mass spectrometer (Thermo Fisher Scientific, Bremen, Germany) coupled with an EASY-nLC 1000 system (Thermo Fisher Scientific, Bremen, Germany). Peptides were separated on a 50 cm × 75 μM ID packed with 2 μM C18 particles (Easy spary column) with a 220 min gradient of solvent B (100% CAN, 0.1% formic acid) form 5% to 40%. Survey MS scans (300–2000 Th) were acquired at a resolution of 70,000 (at m/z 200) with an automated gain control (AGC) target value of 1.0×10^6 and a maximum ion injection of 20 ms. The maximal ion injection time for MS/MS was set to 60 ms at a resolution of 17,500. Dynamic exclusion times were set to 30 s.

2.12. Raw data processing for mass spectrometrical (MS) analysis

The MS/MS spectra were searched with open source software MaxQuant (v. 1.5.1.2) [34] against the Uniprot-human-reference (released in April 2014). A false discovery rate (FDR) cutoff of 1% was applied at the proteins and peptides with minimum peptide length of 7 amino acids. Cysteine carbamidomethylation was set as fixed modification, whereas N-terminal protein acetylation and methionine oxidation were set as variable modifications. The software MaxLFQ, a generic method for label-free quantification was used for relative quantification [35]. In addition, the "match between runs" feature was implemented to increase the number of peptides that can be used for quantification. We stringently filtered our data by requiring a minimum peptide ratio count of 2 in MaxLFQ. Statistical analysis was carried out by Perseus software (v.1.5.0.31, http://www.perseus-framework.org). Each LFQ intensities were transformed by log2 values. Statistical quantification analysis of log-transform data was performed using two sample *t*-test (p value < 0.05). Additionally, in case missing value was existed, we performed the relative quantification of proteins extracted from one group which have a missing value and average of other group which have no missing value. Consequently, Proteins with expression greater than ± 1.5 fold change were added to differentially expressed proteins (DEP). The resulting significant differentially expressed proteins were analyzed for further annotation enrichments using DAVID software exploring cellular processes, pathways, and biological processes.

2.13. Measurement of enzyme activity of mitochondrial respiratory chain

Mitochondrial complexs activity were measured as previously described [36,37]. To prepare sub-mitochondrial particles, isolated mitochondrial pellets were suspended in hypotonic buffer (25 mM potassium phosphate, pH 7.2, 5 mM MgCl2) and then frozen and thawed for three times. The mitochondrial protein concentration was measured using the Bradford assay with BSA as a standard. Complex I activity (NADH:CoQ oxidoreductase) was measured in the presence of decylubiquinone as the rotenone-sensitive decrease in NADH at 340 nm. The activity of Complex II (succinate:DCIP oxidoreductase) was measured in the presence of decylubiquinone plus rotenone as the antimycin A-sensitive reduction of 2,6-DCIP at 600 nm, with 520 nm as the reference wavelength. Complex III activity (Ubiquinol: cytochrome *C* oxidoreductase) was measured in the presence of rotenone and decylubiquinol following the rate of reduction of cytochrome *C* at 550 nm, with 580 nm as the reference wavelength. Complex IV activity (Cytochrome *C* oxidase) was measured as the disappearance of reduced cytochrome *C* at 550 nm. All absorbance measurements were performed in a Beckman DU650 (Beckman Coulter, Fullerton, CA) spectrophotometer. Complex V is assayed in the reverse direction, as F1-ATPase. The assay relies on linking the ATPase activity to NADH oxidation. Complex V activity was measured in as the change in NADH at 340 nm absorbance.

2.14. Blue native polyacrylamide gel electrophoresis (BN-PAGE)

BN-PAGE was performed using the NativePAGE Novex® Bis-Tris Gel system (Invitrogen) according to the manufacturer's instructions. Briefly, 50 μg of isolated mitochondria was solubilized using NativePAGE sample buffer supplemented with 0.5% n-dodecyl-β-D-maltoside. After 30 min incubation on ice, the suspensions were centrifuged at 20,000 × *g* for 10 min at 4 °C. The resulting supernatants

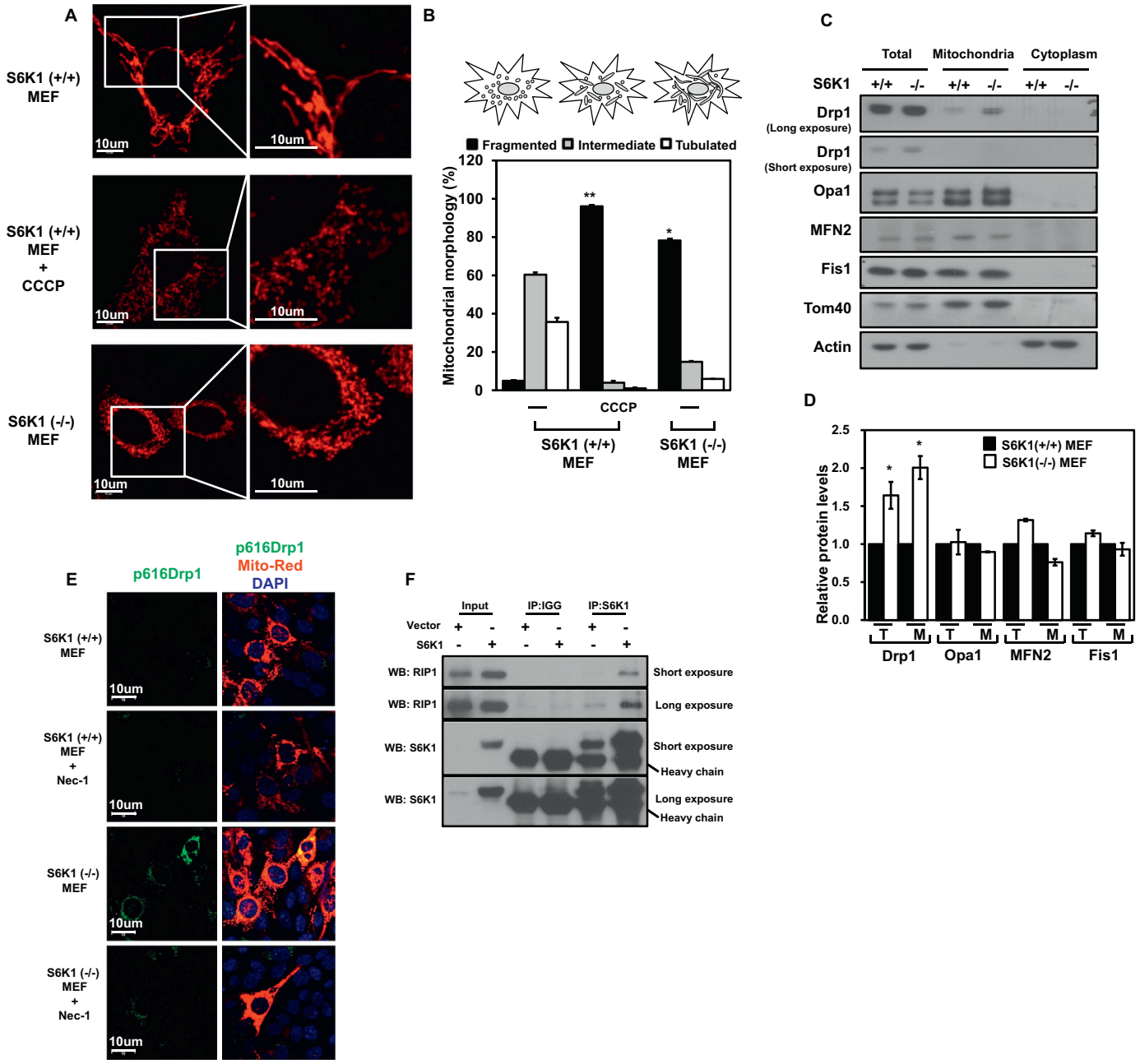

Fig. 1. Morphological changes of mitochondria in S6K1-WT MEFs and S6K1-KO MEFs.(A) S6K1-WT MEFs and S6K1-KO MEFs were transiently transfected with pDsRed–Mito for 48 h. Mitochondrial morphology of cells was monitored by using confocal microscopy. For positive control, S6K1-WT MEFs were treated with 30 μM CCCP for 8 h. These results are a representative of three independent experiments. Scale bars represent 10 μM. (B) Fifty cells of each condition were counted and quantified as the following. (Fragmented; mainly small and round mitochondria, Intermediate; mixture of round and tabulated mitochondria, Tubulated; long and higher interconnected mitochondria). The results are mean ± S.D. of three independent experiments. Asterisk, $p < 0.05$; double asterisk, $p < 0.01$. (C) Mitochondrial fraction from S6K1-WT MEFs and S6K1-KO MEFs were isolated. Regulatory proteins for mitochondria dynamics, fission -related (Drp1 and Fis1) and fusion-related (Opa1 and MFN2) proteins were monitored by immunoblotting. These results are a representative of three independent experiments. (D) Relative densities were obtained by densitometry. Relative expression of total protein was calculated by normalizing densitometric values to that of actin in each lane. For the relative expression of mitochondria-localized protein were normalized with densitometric values of Tom40 in each lane. The results are mean ± S.D. of three independent experiments. Asterisk, $p < 0.05$. (Tot: total, Mito: mitochondria). (E) S6K1-WT MEFs and S6K1-KO MEFs were transiently transfected with pDsRed–Mito for 48 h. The cells were treated with 50 μM Nec-1 for 3 h and processed immune fluorescence assay to detect p616 Drp1. These results are a representative of three independent experiments. Scale bars represent 10 μM. (F) HEK293 cells were plated and transfected with empty control or pcDNA3.1 Myc-S6K1 vectors. After 48 h transfection, cells were harvested and followed by immunoprecipitation assay to check S6K1-Rip1 interaction. These results are a representative of three independent experiments.

were loaded onto a NativePAGE Novex 3–12% Bis-Tris gel. After running, the gel was transferred to a PVDF membrane using the iBlot TM Gel Transfer System (Invitrogen). The membrane was fixed with 8% acetic acid and washed with distilled water. After overnight drying, the membrane was de-stained with methanol and incubated in blocking solution for 30 min at room temperature. For BN-PAGE, the Anti-OXPHOS Complex Kit (Invitrogen) primary antibody cocktail was used. After incubation in the primary antibody dilution, the membrane was

washed and detected using the WesternBreeze® (Invitrogen) Chromogenic Western Blot Immunodetection Kit according to the manufacturer's instructions.

2.15. Analysis for oxygen consumption rate

The mitochondrial oxygen consumption rate (OCR) was measured using a Seahorse XF-24 extracellular flux analyzer (Seahorse Bioscience). On the day before the experiment, the sensor cartridge was placed into the calibration buffer supplied by Seahorse Bioscience and incubated at 37 °C in a non-CO_2 incubator. MEFs were cultured on Seahorse XF-24 plates at a density of 20,000 cells per well. Cells were washed and incubated with assay medium (DMEM without bicarbonate) at 37 °C in a non-CO_2 incubator for 1 h. All media and injection reagents were adjusted to pH 7.4 on the day of the assay. Three baseline measurements of OCR were taken before sequential injection of mitochondrial inhibitors. Three readings were taken after each addition of mitochondrial inhibitor before injection of the subsequent inhibitors. The mitochondrial inhibitors used were oligomycin (2 μg/ml), CCCP (5 μM), and rotenone (1 μM). OCR was automatically calculated and recorded by the Seahorse XF-24 software. After the assays, the plates were saved, and protein levels were measured for each well to confirm equal cell numbers per well. The percentage of change compared with basal rates was calculated as the value of the change divided by the average value of baseline readings.

2.16. ATP measurement

Cells were seeded in 12 well plate overnight. 2DG, 2DG + Oligomycin were individually treated to the cells for 3 h then lysed the cell with 100 ul of luciferase lysis buffer (Invitrogen). Reaction was performed by adding 10 ul of samples into 90 ul of ATP solution-supplied by Invitrogen and measured ATP level using Luminometer Lumat LB 9507. By using 2-DG and oligomycin, the ratio of ATP production between glycolysis-dependent and OxPhos system-dependent ATP production was calculated. Oligomycin blocks proton channels, resulting the inhibition of OxPhos system-dependent ATP production while 2-DG blocks glycolysis-dependent ATP production. The intracellular ATP were calculated as follows: Glycolytic ATP (ATP_{gly}) = total ATP − ATP_{2DG}, OxPhos ATP under 2DG treatment (ATP_{OxPhos}) = ATP_{2DG} − $ATP_{2DG+Oligo}$.

2.17. Statistical analysis

Data are expressed as the mean ± S.E. from at least three separate experiments. The differences between groups were analyzed using a Student's *t*-test and $P < 0.05$ is considered statistically significant. Quantitative analyses of the western blotting results were performed by using Image J software (version 1.45).

3. Results

3.1. Mitochondrial fission is upregulated in S6K1 knockout mouse embryonic fibroblast (MEFs)

Earlier studies [38] indicated that S6K1 regulates mitochondrial dynamics in the HeLa cells. In order to further define this phenomenon in the normal cells, S6K1-knockout (KO) MEFs were employed as previously described [39]. The mitochondria of S6K1-WT MEFs and S6K1-KO MEFs were labeled with Mito-Red (pDs-Red Mito). As shown in Fig. 1A, the mitochondrial fragmentation was elevated in S6K1-KO MEFs compared to wild-type controls, and reached a level similar to wild-type MEFs treated with CCCP a mitochondrial uncoupler, which is a mitochondrial fragmentation inducer [40]. Based on the mitochondrial morphology, the cells were categorized as (1) fragmented-mainly small and round mitochondria, (2) intermediate-mixture of round and tubulated mitochondria or (3) tubulated-long and higher interconnected mitochondria (Fig. 1B). A marked increase in the number of fragmented mitochondria was detected in S6K1-KO MEFs compared to S6K1-WT MEFs indicating that the absence of S6K1 leads to mitochondria fission in these cells. To further elucidate the link between S6K1 and regulatory proteins for mitochondria dynamics, fission -related (Drp1 and Fis1) and fusion-related (Opa1 and MFN2) proteins were characterized. Total Drp1 and mitochondria-localized Drp1 (a key regulator of mitochondrial fission) were elevated in S6K1-KO MEFs compared to S6K1-WT MEFs (Fig. 1C, top two panel, Fig. 1D). There was no detectable changes of other regulatory proteins, suggesting that Drp1 is involved in S6K1-medated mitochondrial dynamics.

It has been shown that the fission activity of Drp1 is tightly regulated by phosphorylation [22]. Phosphorylation of Drp1 on Ser-616 activates Drp1 activity while Ser-637 phosphorylation inhibits [24]. Both whole-cell and mitochondrial extracts demonstrated higher levels of Drp1 Ser-616 phosphorylation, suggesting that S6K1-regulted Drp1 activity may be important for mitochondria fission whereas Ser-637 phosphorylation of Drp1 was not altered in both conditions (Supplement Fig. 1). The enhancement of Drp1-mediated fission was observed by Rip1 activation previously {Wang, 2014 #186}. Nec-1, the kinase inhibitor of Rip1 decreased Rip1-regulated Drp1 phosphorylation at Serine 616, consequently leading to the defection in fission. In order to evaluate the possibility if S6K1-mediated Drp1 regulation is dependent on Rip1, immunofluorescence analysis of S6K1-WT MEFS and S6K1-KO MEFs with anti-Ser-616 Drp1 antibody following Nec-1 treatment was employed (Fig. 1E). The expression and mitochondrial localization of phosphor-Ser-616 Drp1 were remarkable enhanced in S6K1 KO-MEFs, indicating that S6K1 actually induced mitochondrial fission by increasing Ser-616 Drp1 phosphorylation. As expected, the treatment of cells with Nec-1 abolished the enhancement of phospho-Ser-616 Drp1 level as well as the mitochondrial co-localization in S6K1-KO MEFs. Hence, S6K1 absence induced phosphor-Ser-616 Drp1 through Rip1 kinase activity. Furthermore, the immunoprecipitation assay revealed that S6K1 bound to Rip1 in both endogenous and exogenous level (Fig. 1F). Taken together, S6K1 interacted with Rip1 and regulate its kinase activity. Once Rip1 is released from this complex such as S6K1 deletion, it phosphorylated Drp1 at serine 616, resulting in mitochondrial fission.

3.2. No detectable changes of autophagy and mitophagy was found in S6K1-KO MEFs

Since mitochondrial fragmentation is considered as an early step of autophagy and mitophagy, we examined changes in these processes in our S6K1-KO MEFs [41]. Treatment of S6K1-WT MEFs with CCCP induced the accumulation of LC3B-II, a marker of autophagy (Fig. 2A). Basal levels of LC3B-II were not altered in S6K1-KO MEFs (Fig. 2A). Importantly, LC3B-II accumulation also increased in these cells following CCCP treatment (Fig. 2A), suggesting that autophagy was not altered by S6K1 depletion. In order to monitor mitophagy, staining for mitochondrial localized- LC3 punctate was performed. There was no detectable over-lapping signal for mitochondria (Mito-Red) and LC3 punctate staining in S6K-KO MEFs, similar to S6K1-WT MEFs (Fig. 2B). Over-lapping staining was, however enhanced in S6K1-WT MEFs treated with CCCP (Fig. 2C). Consistent with these results, mitochondrial recruitment of exogenously expressed GFP-Parkin was detected in both S6K1-WT MEFs and S6K1-KO MEFs treated with CCCP (Fig. 2D and E). Taken together, these data suggest that the depletion of S6K1 does not influence autophagy and mitophagy in MEFs, despite the enhanced mitochondrial fission in S6K1-KO MEFs.

3.3. Mitochondrial respiratory capacity is enhanced in S6K1-KO MEFs with a reduction of mitochondrial mass

Mitochondrial morphology closely links with its capacity and

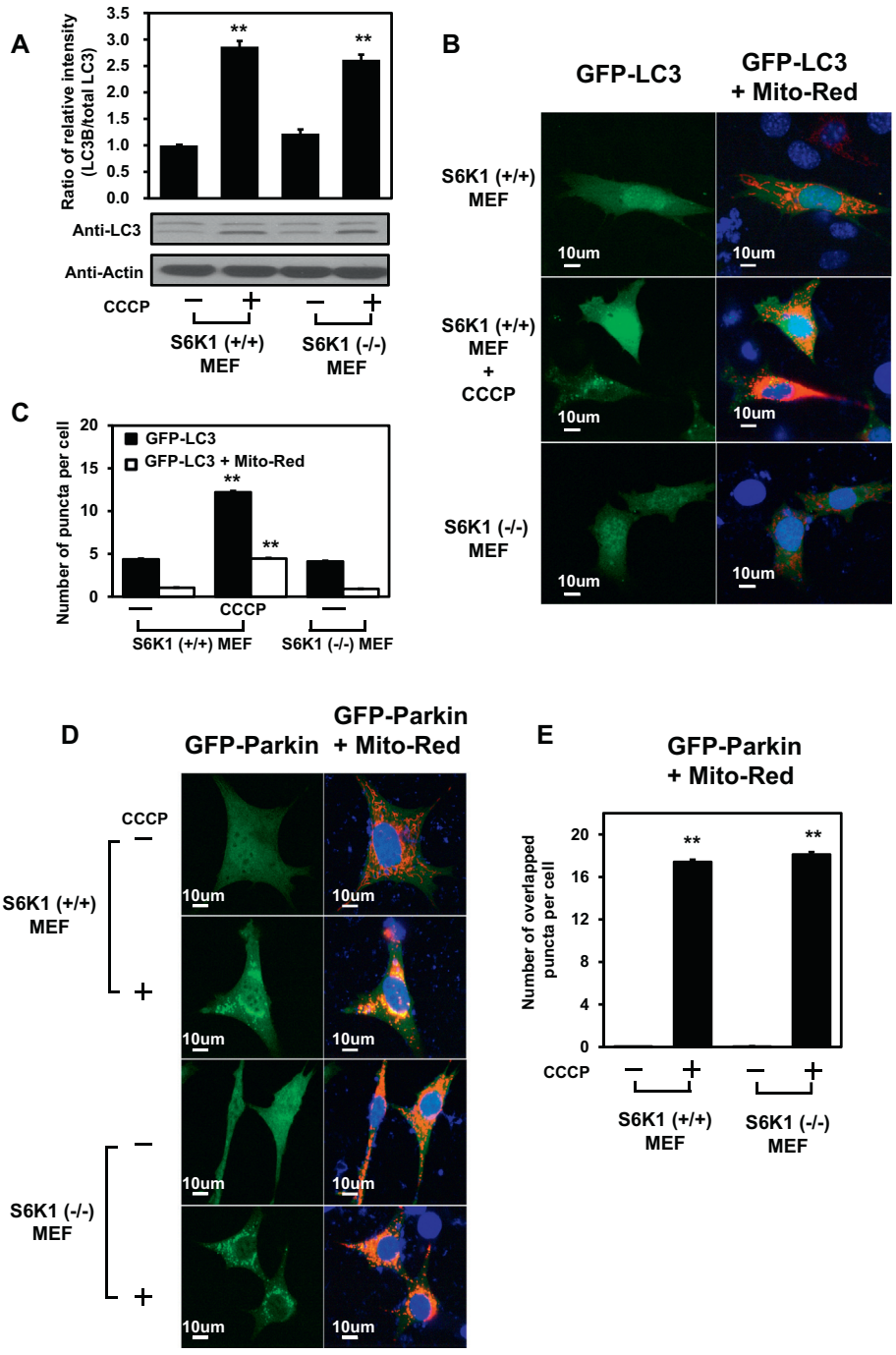

Fig. 2. Effects of S6K1 on autophagy and mitophagy in S6K1 WT MEFs and S6K1-KO MEFs. (A) S6K1-WT MEFs and S6K1-KO MEFs were treated with 30 μM CCCP for 8 h. Total cell lysate were analyzed by western blot analysis with anti-LC3B and anti-actin antibody (lower panel). The results represent the levels of autophagy by calculating the intensity ratio between LC3B-II and total LC3B. Relative intensity of each band was calculated by normalizing densitometric values to that of actin in each lane. The results are mean ± S.D. of three independent experiments. Asterisk, $p < 0.05$; double asterisk, $p < 0.01$. (B) S6K1-WT MEFs and S6K1-KO MEFs were cotransfected with Mito-Red and GFP-LC3B for 48 h. The samples was analyzed by confocal microscope. Red fluorescence represented for mitochondria, Green fluorescence represented for LC3B and Blue fluorescence DAPI represented for nucleus. These results are a representative of three independent experiments. Scale bars represent 10 μM. (C) The results was calculated as a number of LC3B puncta per cell (black bar), or merged LC3B puncta with Mito-Red per cell (white bar). Fifty cells were analyzed for each sample. The results are mean ± S.D. of three independent experiments. Asterisk, $p < 0.05$; double asterisk, $p < 0.01$. (D) S6K1-WT MEFs and S6K1-KO MEFs were co-transfected with Mito-Red and GFP-Parkin for 48 h. The sample was analyzed by confocal microscope. These results are a representative of three independent experiments. Scale bars represent 10 μM. (E) The results was calculated as a number of merged GFP-parkin puncta with Mito-Red per cell. Fifty cells were analyzed for each condition. The results are mean ± S.D. of three independent experiments. Asterisk, $p < 0.05$; double asterisk, $p < 0.01$. (For interpretation of the references to color in this figure legend, the reader is referred to the web version of this article.)

function [29,42,43]. Therefore the mitochondrial function in S6K1-KO MEFs was analyzed, since S6K1-KO MEFs demonstrated mitochondrial fission without increased mitophagy (Figs. 1 and 2). Interestingly, mitochondrial membrane potential (ΔΨm; mitochondrial respiratory capacity) was elevated in S6K1-KO MEFs compared to control cells (Fig. 3A). The ΔΨm of both MEF subtypes was significantly reduced to the similar extend following CCCP treatment (Fig. 3B). Transmission electron microscopy (TEM) images of S6K1-KO MEFs showed less mitochondria than S6K1-WT MEFs (Fig. 3C). Relative mitochondrial mass of S6K1-KO MEFs was only 50 % in S6K1-WT MEFs (Fig. 3D and E). These results indicated that mitochondrial respiratory capacity of S6K1-KO MEFs was enhanced with the reduction of mitochondria mass, compared to wild type MEFs, suggesting that mitochondria function is actually elevated in the absence of S6K1. To test this hypothesis, in vitro OxPhos activity and oxygen consumption rate were measured. Using blue native polyacrylamide gel electrophoresis (BN-PAGE), multiple complexes for OxPhos were not increased in S6K1-KO MEFs (Fig. 3F). S6K1-KO MEFs exhibited higher OxPhos complex II activity with no changes in complexes I, III, IV or V detected (Fig. 3G). In addition, the oxygen consumption rate (OCR) was enhanced in S6K1-KO MEFs compared to S6K1-WT MEFs (Fig. 3H). These results suggested that S6K1 depletion did not affect mitochondrial respiratory chain assembly but was able to modulate the respiration activity which might due to the changes in OxPhos components (subunit proteins, coactivators, substrates/products homeostasis) and/or in mitochondrial morphology.

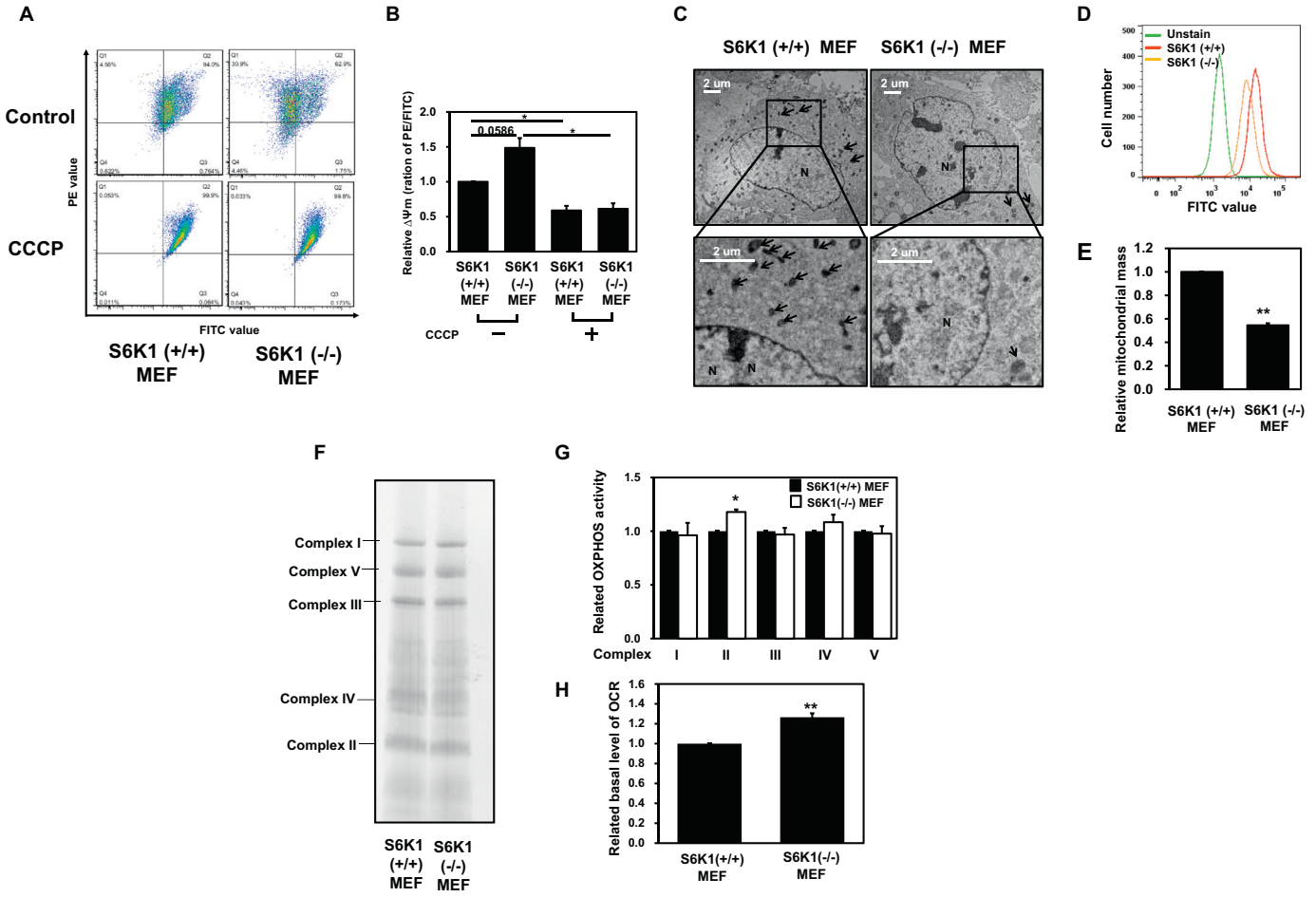

Fig. 3. Analysis of mitochondria-related parameters in S6K1 WT MEFs and S6K1-KO MEFs. (A) S6K1-WT MEFs and S6K1-KO MEFs were treated with or without 30 μM CCCP for 10 min, followed by staining with JC-1 dye. Mitochondrial membrane potential was measured using flow cytometry. These results are a representative of three independent experiments. (B) Relative and statistical differences of mitochondrial membrane potential (ratio of Q2/Q3) was calculated and set the values for S6K1-WT MEFs as 1. The results are presented as means ± S.D. of three independent experiments. Asterisk, $p < 0.05$; 0.0586, $p = 0.058601$. (C) S6K1-WT MEFs and S6K1-KO MEFs were analyzed by Transmission Electron Microscopy. Black Arrows: mitochondria; N: nucleus. These results are a representative of three independent experiments. Scale bars represent 2 μM. (D) The cells were stained MitoTracker Green FM dye for mitochondria mass. Mitochondria mass were measured by flow cytometry. These results are a representative of three independent experiments. (E) Relative mitochondrial mass was calculated and set values for S6K1-WT MEFs as 1. The results are presented as means ± S.D. of three independent experiments. Asterisk, $p < 0.05$; double asterisk, $p < 0.01$. (F) Mitochondrial fraction was isolated from S6K1-WT MEFs and S6K1-KO MEFs. Samples were analyzed by using BN-PAGE to detect the each OxPhos complexes. (G) Isolated mitochondria from both MEFs was incubated with the corresponding inhibitors to measure the each OxPhos-complex activity as the described in the materials and methods. The results are mean ± S.D. of three independent experiments. Asterisk, $p < 0.05$. (H) S6K1-WT MEFs and S6K1-KO MEFs were plated in DMEM media for 24 h. Oxygen consumption rate (OCR) was determined by using Seahorse XF-24 extracellular flux analyzer. The results are presented as means ± S.D. of three independent experiments.

3.4. Proteomic analysis for mitochondrial proteins supported the elevation of mitochondrial respiratory capacity in S6K1-KO MEFs

Proteomic analysis of isolated mitochondria from S6K1-WT MEFs and S6K1-KO MEFs has been performed to investigate the possible mechanism how mitochondria function is elevated in S6K1-KO MEFs. Following the analysis of identified proteins from mitochondrial fraction of both cell types, as shown in the schematic diagram (Fig. 4A), 1372 mitochondrial proteins were identified among 4519 detectable proteins (Fig. 4B, top panel) which were enriched for mitochondrial proteins, confirming the integrity of the mitochondrial preparation (Fig. 4B, bottom panel), indicating that mitochondrial fraction has been prepared properly. Heat-map analysis of differentially expressed proteins between S6K1-WT MEFs and S6K1-KO MEFs revealed that the electron transport chain, oxidation-reduction, metabolic cofactors, metabolic coenzymes and fatty acid metabolic proteins were highly upregulated in mitochondria from S6K1-KO MEFs whereas proteins involved in ATP metabolic process were down-regulated (Fig. 4C). Furthermore, a network model of OxPhos complex subunits from the detectable proteins of complexes (complex I: 34 proteins, complex II: 4 proteins, complex III: 7 proteins, complex IV: 10 proteins and complex V: 24 proteins) showed that majority of subunit proteins in complex I, II, III and IV were significantly increased (complex I: 68%, II: 75%, III: 86%, IV: 80%). Overall, these findings suggest that S6K1-KO MEFs displayed a higher respiratory activity due to an elevation of OxPhos component.

3.5. Glycolytic ATP production was increased while OxPhos ATP production was not changed in S6K1-KO MEFs

Since mitochondrial activity were elevated in S6K1-KO MEFs, intracellular ATP production was monitored by using several inhibitors as described in the materials and methods. S6K1 depletion enhanced total ATP levels compared to controls (Fig. 5A). Interestingly, glycolytic ATP production was increased in S6K1-KO MEFs while OxPhos ATP production was not altered (Fig. 5A and B). Consistent with these

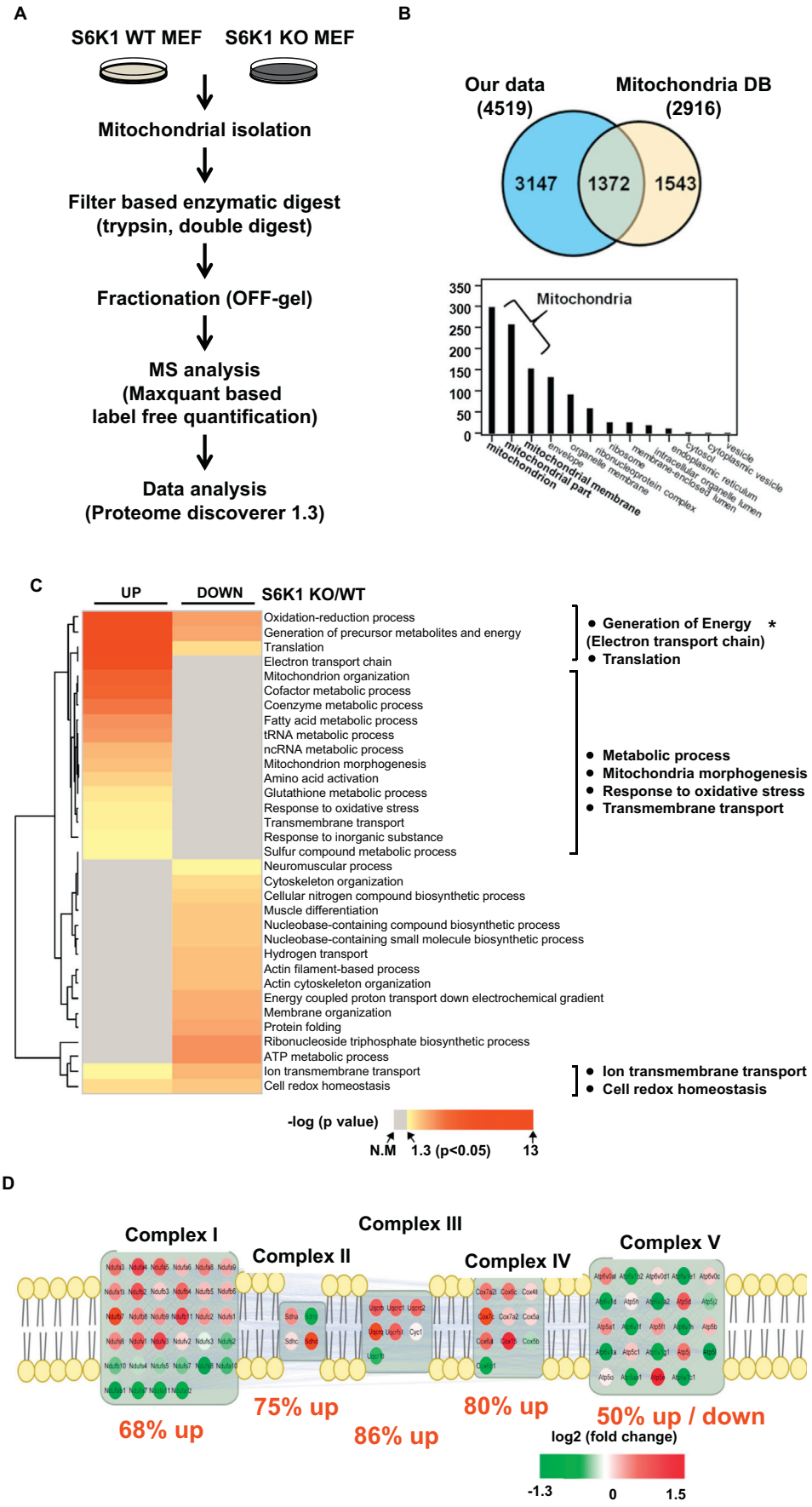

Fig. 4. Comparison of mitochondrial proteomes between S6K1-WT MEFs and S6K1-KO MEFs (A) The schematic diagram for the proteomic analysis of isolated mitochondria from S6K1-WT MEFs and S6K1-KO MEFs. Isolated mitochondria proteins were digested and analyzed by Bench top orbitrap mass spectrometry (Q-Exacitve). MaxLFQ, based on MS1 level quantification, was used. (B) Enrichment of mitochondria proteins from 3-known mouse mitochondria proteome database were used for the further analysis. The cellular component proteins identified from proteomic analysis were confirmed by DAVID bioinformatics tool. The enrichment factors (count) were shown for proteins from 1372 mitochondria proteins. (C) Heat-map shows significant GO biological process terms (p-value < 0.05) for differentially expressed proteins between S6K1-WT mitochondria and S6K1-KO mitochondria. Color bar represents the gradient $-\log^{10}$ (p-value).The term with red color indicates critical alteration in S6K1-KO MEFs. Star markings show the most enriched GO category in a heat-map. (D) A network model of OxPhos complex subunits. Almost all proteins of complex I (34-genes), complex II (4-genes), complex III (7-genes), complex IV (10 -genes) and complex V (24-genes) were identified. Complex I-IV proteins were upregulated overall and complex V don't have distinctive direction of alteration. Color bar indicates gradient of $\log^2$ fold change. All are indicated by gene symbol. (For interpretation of the references to color in this figure legend, the reader is referred to the web version of this article.)

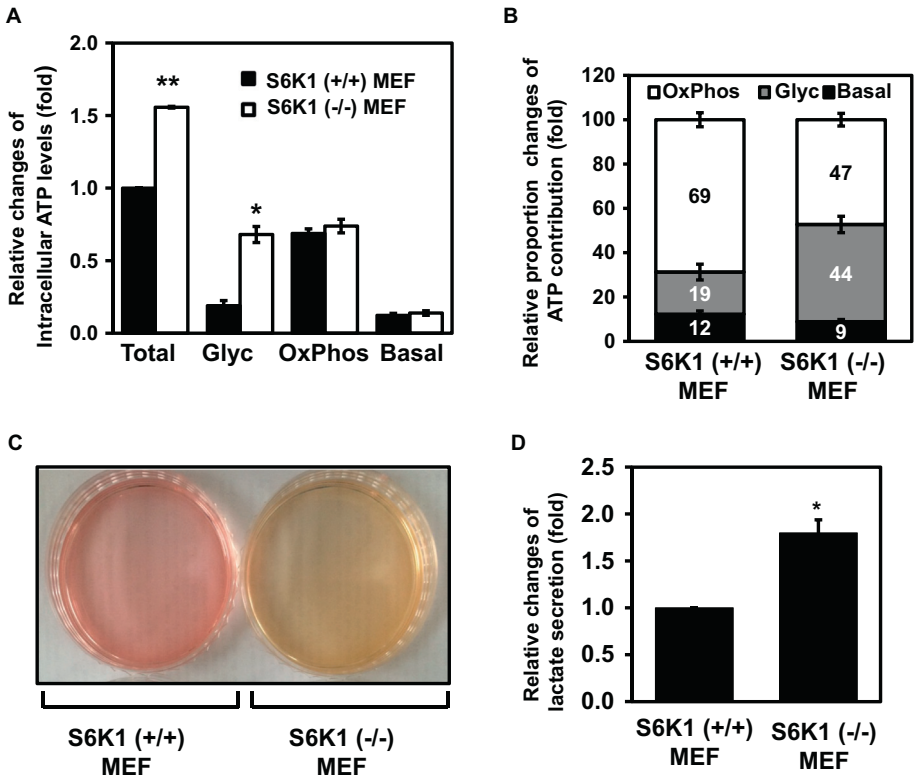

Fig. 5. Effects of S6K1 depletion on the energy metabolism (A) S6K1-WT MEFs and S6K1-KO MEFs were plated and pretreated with 2DG or 2DG/Oligomycin for 3 h. ATP level then was measured using ATP kit guideline from Invitrogen. Glycolysis-dependent ATP (Gly), OxPhos-dependent ATP (OxPhos) and basal (Basal) ATP were calculated as the described in the materials and methods. The results are mean ± S.D. of three independent experiments. (B) Proportion of ATP contribution was calculated. 2DG-sensitive (glycolysis-dependent; Gly) and Oligomycin-sensitive (OxPhos-dependent; OxPhos) ATP production were indicated as a percentage of total cellular ATP level. (C) After 48 h incubation of both MEFs, the acidification of cell culture medium was imaged. These results are a representative of three independent experiments. (D) Lactate levels in culture-media were measured by using lactate assay kit. The results are mean ± S.D. of three independent experiments. Asterisk, $p < 0.05$; double asterisk, $p < 0.01$.

observation, the pH of culture medium indicated that the medium of S6K1-KO MEFs was more acidic than that of S6K1-WT MEFs (Fig. 5C). As expected, the secretion of lactic acid was also increased in S6K1-KO MEFs (Fig. 5D), indicating that the energy metabolism has been shifted to glycolytic dependent pathways in S6K1-KO MEFs.

3.6. S6K1-mediated mitochondrial fission and mitochondrial functions were positively regulated by Drp1 activity

Based on previous results (Figs. 3–5), elevated ΔΨm and mitochondrial activity does not appear to contribute to OxPhos ATP production in S6K1-KO MEFs. Therefore the possible involvement of Drp1-regulated mitochondrial fission was examined by using Drp1 inhibitor, Mdivi1. Mitochondrial fission in S6K1-KO MEFs was blocked by the treatment of cells with Mdivi1 (Fig. 6A). ΔΨm of Mdivi1-treated S6K1-KO MEFs was also reduced (Fig. 6B), resulting to the elevation of OxPhos ATP production (Fig. 6C), suggesting that Drp1 activity is required for S6K1 absence-mediated mitochondrial functions. Moreover, treatment of Nec-1, a Rip1 inhibitor, which also inhibited Drp1-mediated fission (Fig. 1E) exposed the similar mitochondrial recovery with Mdivi1 treatment. After normalizing with non-treated cells respectively, the relative ΔΨm in Nec-1 treated-S6K1 KO MEFs was only 0.6 while this value in Nec-1 treated-S6K1 WT MEFs was almost 1 (Fig. 6D). Furthermore, Nec-1 treatment significantly increased OxPhos ATP in S6K1 KO MEFs indicating for the elevation of coupling activity (Fig. 6E).

4. Discussion

Mitochondria represent a key cellular organelles and utilize both vital and lethal functions in physiological and pathological settings [5,42–44]. The role of mitochondria in cell signaling and energy metabolism is closely associated with its morphology. Fission, one of two mitochondrial dynamic controlling processes was found to be upregulated in S6K1-KO MEFs (Fig. 1). Fission is shown to be under control of Drp1 modification as well as trans-localization of Drp1 [25]. S6K1 is a member of the AGC family of serine/threonine protein kinases [45,46], well known as an effector of mTOR in insulin and nutrient signaling [38] as well as in many cellular processes including mRNA splicing and transcription [45]. In addition, mitochondrial morphology and function are tightly associated with obesity and diabetes [47,48]. Interestingly, it has been reported that the absence of S6K1 in mice protected against age- and diet-induced obesity with the enhancement of insulin sensitivity [28]. However the morphological role of mitochondria in these mice was not investigated in details. Here we reported that S6K1 deficiency induced Drp1-mediated fission, thereby affecting the cellular energy metabolism. Mitochondrial fission induced by S6K1 depletion reduced the efficiency of OxPhos ATP production (Figs. 4 and 5), suggesting that these events might be important mechanism to explain the protective phenotype of S6K1-KO mice against obesity when they were fed with high fat diet. Therefore these results have provided a new insight into the role of S6K1 in regulating mitochondrial function and structure in cells.

In the life cycle of mitochondria, it frequently is faced to the danger condition such as ROS, mtDNA mutation, low mitochondrial membrane potential and Ca^{2+} overload [49,50]. The mitochondrial quality control, mediated by mitophagy, is highlighted as an emerging topic involved in cell development and diseases. In this process, mitochondrial fission is considered as an earlier event, dividing weak mitochondria into one healthy and one damage mitochondria, which recruits autophagosome by conjugating with LC3. Consequently, damaged mitochondria will be removed by fusing with lysosome [29]. Based on the previous study [38] and Fig. 1, a question has been raised if S6K1-mediated fission can consequently increase autophagy and mitophagy since mTOR activity controlled the early stage of autophagy? However, the autophagic and mitophagic events were not affected in S6K1-KO MEFs (Fig. 2). Interestingly, ΔΨm, which is an indicator of healthy mitochondria, was enhanced in S6K1-KO MEFs compared to S6K1-WT MEFs (Fig. 3A and B), suggesting that S6K1 depletion was able to induce the mitochondrial fission and maintain the hyperpolarization of

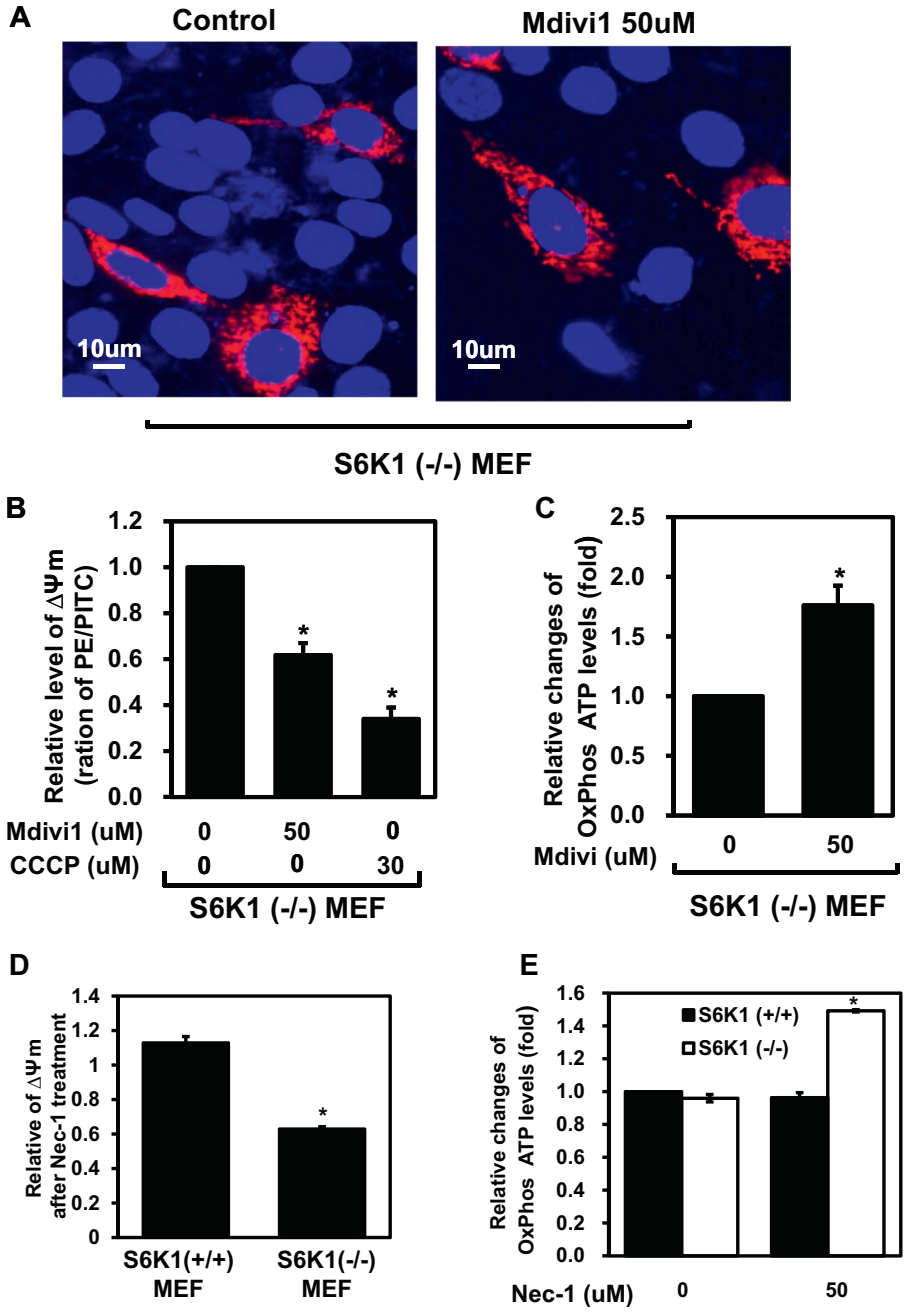

Fig. 6. Reversion of mitochondrial functions by returning the mitochondrial morphology in S6K1-KO MEFs. (A) S6K1-KO MEFs were transiently transfected with pDsRed–Mito for 48 h. The cells were treated with 50 μM Mdivi-1 for 30 mins. Mitochondrial morphology of cells was monitored by using confocal microscopy. These results are a representative of three independent experiments. Scale bars represent 10 μM. (B) S6K1-KO MEFs were treated with 50 μM Mdvidi-1 for 30 mins or 30 μM CCCP for 10 mins, followed by staining of cells with JC-1 dye. Mitochondrial membrane potential was measured using flow cytometry. Relative and statistical differences of mitochondrial membrane potential (ratio of Q2/Q3) were calculated and set the values for untreated control as 1. The results are mean ± S.D. of three independent experiments. Asterisk, $p < 0.05$; double asterisk, $p < 0.01$. (C) The cells were treated with 50 μM Mdivi-1 for 30 mins. OxPhos-dependent ATP was measured as the described previously. OxPhos ATP value in the untreated cells was set as 1. The results are presented as means ± S.D. of three independent experiments. Asterisk, $p < 0.05$; double asterisk, $p < 0.01$. (D) S6K1-KO MEFs were treated with 50 μM Nec-1 for 3 followed by staining of cells with JC-1 dye. Mitochondrial membrane potential was measured using flow cytometry. Relative and statistical differences of mitochondrial membrane potential (ratio of PE/FITC) were calculated and set the values for untreated control in both S6K1 WT/KO MEFs as 1. The results are mean ± S.D. of three independent experiments. Asterisk, $p < 0.05$; double asterisk, $p < 0.01$. (E) The cells were treated with 50 μM Nec-1 for 3 h. OxPhos-dependent ATP was measured as the described previously. OxPhos ATP value in the untreated cells was set as 1. The results are presented as means ± S.D. of three independent experiments. Asterisk, $p < 0.05$; double asterisk, $p < 0.01$.

mitochondria even though the autophagy and mitophagy were not occurred in these cells.

During the glucose metabolism, once glucose is imported to the cell, it will be metabolized, then produce ATP and pyruvate in cytoplasm. The flows of generated pyruvate form a junction. Pyruvate from glycolysis may turn into the lactate pathway. The enhancement of glucose uptake and glycolysis leads to higher level of pyruvate, consequently increase the activity of lactate pathway and lactic acid production. On the other hand, cytosolic pyruvate may be entered to mitochondria via pyruvate carriers and become a substrate for TCA cycle. In this regards, S6K1-KO MEFs showed the preference of lactate metabolism (Fig. 5C and D) to generate ATP without the alteration of OxPhos ATP production (Fig. 5A) in these cells. Interestingly, the mitochondrial respiratory capacity, monitored by OxPhos complex activity (Fig. 3G), oxygen consumption rate (OCR; Fig. 3H) and proteomic analysis of mitochondrial fraction (Fig. 4), were enhanced in S6K1-KO MEFs compared to the control MEFs whereas the consequent OxPhos-dependent ATP production was not changed (Fig. 5A). These observation can be explained by the fission form of mitochondria which may have lower ATP productive yield. Indeed, Molina and colleagues have shown that hyperpolarized mitochondrial fission was also observed in the cells with the nutrient overload [48]. Similarly, the elongated mitochondria were found as a protection event against starvation [51,52]. These raise a hypothesis that the changes of mitochondrial morphology are consequent events of energy adaption. The balance of nutrient supply and energy demand is associated with corresponding changes to mitochondrial morphology and to bioenergetics efficiency [29]. Previously it has been reported that PKB activation, which can be elevated by S6K1 absence [28], increased glucose uptake by modulating GLUT4 traffic [53,54]. High glucose uptake is considered as nutrient access condition, which breaks the energetic balance, enhances the OxPhos activity and promotes mitochondrial fission [29]. In consistent with

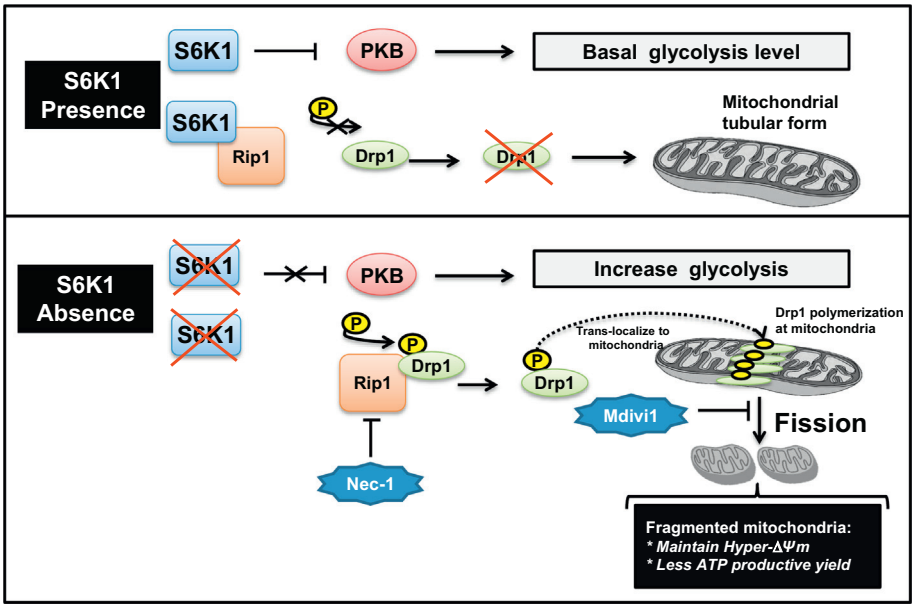

Fig. 7. The proposed model for S6K1 function in mitochondria function and energy metabolism. S6K1 regulates PKB activation via negative feedback pathway hereby maintaining glycolysis at basal level. In addition, S6K1 interacts with Rip1 and inhibits Rip-mediated Drp1 phosphorylation at Serine 616. Once S6K1 is lacked, PKB is hyper activated resulting in the enhancement of glycolysis. S6K1 absence facilitates Rip1-mediated Drp1 phosphorylation, consequently increases mitochondrial Drp1 and mitochondrial fission. Fragmented mitochondria maintained a high mitochondrial membrane potential and reduced ATP production. Thus S6K1 deficiency increased glycolysis-dependent ATP production but not OxPhos-dependent ATP production, due to the change of mitochondrial morphology and function. Recovery of tubular mitochondria by Nec-1 or Mdvi1 in S6K1 KO MEFs also returns the mitochondrial function. This tubulated mitochondria could have a strong ability to generate ATP, finally reduced mitochondrial membrane potential.

these observations, S6K1-KO MEFs showed a higher mitochondrial fission (Fig. 1), a hyperpolization of ΔΨm (Fig. 3A and B) and an elevation of total ATP level (Fig. 5A). In addition, Drp1 phosphorylation on S616 (the active form of Drp1) was appeared to be high in S6K1-KO MEFs (Supplemental Fig. 1). Rip1, the upstream kinase which could phosphorylate Drp1 at Serine 616 interacted with S6K1. The elevations of pS616 Drp1 level and its translocation to mitochondria in S6K1 KO MEFs were depressed by treating with Nec-1 a kinase inhibitor of Rip1. Furthermore the restoration of tubular form of mitochondria in S6K1-KO MEFs by Mdivi1 treatment (Drp1inhibitor) or Nec-1 treatment (rip1 inhibitor) lead to decrease ΔΨm and increase OxPhos ATP production (Fig. 6), indicating that S6K1 depletion-induced mitochondrial fission event might be the molecular mechanism to maintain the hyperpolization of ΔΨm and reduce the efficiency of OxPhos-dependent ATP production (Fig. 7). Taken together, these results have proposed a potential role of S6K1 in energy metabolism by modulating mitochondrial respiratory capacity and mitochondrial morphology.

Conflict of interest

The authors declare that there are no conflicts of interest.

Author contributions

Q.T., J.H.J., K.P.K, M.H.C. and J.P. contributed to concept of this study and planned all the experiments; Q.T., J.P., H.L., Y.H., and H.C. performed all the experiments; Q.T., M.K. and S.P. conducted the confocal microscopic analysis. S.H., S.H.K., D.P.B. and G.T. gave an extensive data interpretation and discussion. J.P. managed the grant and wrote the manuscript. All authors reviewed the manuscript.

Acknowledgement

This work was financially supported by the National Research Foundation of Korea (NRF) grant funded by the Korea Government (NRF-2012M3A9B6055302, NRF-2015R1A2A2A01003597, NRF-2015R1D1A3A01015694, NRF-2016K1A3A1A08953546).

References

[1] G. Kroemer, L. Galluzzi, C. Brenner, Physiol. Rev. 87 (2007) 99–163.
[2] P. Mitchell, J. Moyle, Nature 213 (1967) 137–139.
[3] L. Galluzzi, N. Joza, E. Tasdemir, M.C. Maiuri, M. Hengartner, J.M. Abrams, N. Tavernarakis, J. Penninger, F. Madeo, G. Kroemer, Cell Death Differ. 15 (2008) 1113–1123.
[4] S.W. Tait, D.R. Green, J. Cell Sci. 125 (2012) 807–815.
[5] L. Galluzzi, O. Kepp, G. Kroemer, Nat. Rev. Mol. Cell Biol. 13 (2012) 780–788.
[6] L.A. Sena, N.S. Chandel, Mol. Cell 48 (2012) 158–167.
[7] D.C. Wallace, Annu. Rev. Genet. 39 (2005) 359–407.
[8] T. Kanki, K. Wang, Y. Cao, M. Baba, D.J. Klionsky, Dev. Cell 17 (2009) 98–109.
[9] K. Okamoto, N. Kondo-Okamoto, Y. Ohsumi, Dev. Cell 17 (2009) 87–97.
[10] I. Novak, V. Kirkin, D.G. McEwan, J. Zhang, P. Wild, A. Rozenknop, V. Rogov, F. Lohr, D. Popovic, A. Occhipinti, A.S. Reichert, J. Terzic, V. Dotsch, P.A. Ney, I. Dikic, EMBO Rep. 11 (2010) 45–51.
[11] R.A. Hanna, M.N. Quinsay, A.M. Orogo, K. Giang, S. Rikka, Gustafsson AB, J. Biol. Chem. 287 (2012) 19094–19104.
[12] L. Liu, D. Feng, G. Chen, M. Chen, Q. Zheng, P. Song, Q. Ma, C. Zhu, R. Wang, W. Qi, L. Huang, P. Xue, B. Li, X. Wang, H. Jin, J. Wang, F. Yang, P. Liu, Y. Zhu, S. Sui, Q. Chen, Nat. Cell Biol. 14 (2012) 177–185.
[13] Y. Kim, J. Park, S. Kim, S. Song, S.K. Kwon, S.H. Lee, T. Kitada, J.M. Kim, J. Chung, Biochem. Biophys. Res. Commun. 377 (2008) 975–980.
[14] D. Narendra, A. Tanaka, D.F. Suen, R.J. Youle, J. Cell Biol. 183 (2008) 795–803.
[15] J. Bereiter-Hahn, M. Voth, Microsc. Res. Tech. 27 (1994) 198–219.
[16] M. Liesa, M. Palacin, A. Zorzano, Physiol. Rev. 89 (2009) 799–845.
[17] S. Campello, L. Scorrano, EMBO Rep. 11 (2010) 678–684.
[18] S. Cipolat, O. Martins de Brito, B. Dal Zilio, L. Scorrano, Proc. Natl. Acad. Sci. U. S. A. 101 (2004) 15927–15932.
[19] A. Santel, M.T. Fuller, J. Cell Sci. 114 (2001) 867–874.
[20] E. Ingerman, E.M. Perkins, M. Marino, J.A. Mears, J.M. McCaffery, J.E. Hinshaw, J. Nunnari, J. Cell Biol. 170 (2005) 1021–1027.
[21] A. Legesse-Miller, R.H. Massol, T. Kirchhausen, Mol. Biol. Cell 14 (2003) 1953–1963.
[22] K. Elgass, J. Pakay, M.T. Ryan, C.S. Palmer, Biochim. Biophys. Acta 2013 (1833) 150–161.
[23] N. Taguchi, N. Ishihara, A. Jofuku, T. Oka, K. Mihara, J. Biol. Chem. 282 (2007) 11521–11529.
[24] C.R. Chang, C. Blackstone, J. Biol. Chem. 282 (2007) 21583–21587.
[25] S.K. Hanks, T. Hunter, FASEB J. 9 (1995) 576–596.
[26] B.D. Manning, A.R. Tee, M.N. Logsdon, J. Blenis, L.C. Cantley, Mol. Cell 10 (2002) 151–162.
[27] T.R. Fenton, I.T. Gout, Int. J. Biochem. Cell Biol. 43 (2011) 47–59.
[28] S.H. Um, F. Frigerio, M. Watanabe, F. Picard, M. Joaquin, M. Sticker, S. Fumagalli, P.R. Allegrini, S.C. Kozma, J. Auwerx, G. Thomas, Nature 431 (2004) 200–205.
[29] M. Liesa, O.S. Shirihai, Cell Metab. 17 (2013) 491–506.
[30] J. Park, H. Lee, Q. Tran, K. Mun, D. Kim, Y. Hong, S.H. Kwon, D. Brazil, J. Park, S.H. Kim, Toxicol. Res. 33 (2017) 63–69.
[31] Y. Li, J. Park, L. Piao, G. Kong, Y. Kim, K.A. Park, T. Zhang, J. Hong, G.M. Hur, J.H. Seok, S.W. Choi, B.C. Yoo, B.A. Hemmings, D.P. Brazil, S.H. Kim, J. Park, Cell. Signal. 25 (2013) 74–84.
[32] J.R. Wisniewski, A. Zougman, N. Nagaraj, M. Mann, Nat. Methods 6 (2009) 359–362.
[33] J.R. Wisniewski, M. Mann, Anal. Chem. 84 (2012) 2631–2637.
[34] J. Cox, M. Mann, Nat. Biotechnol. 26 (2008) 1367–1372.
[35] J. Cox, M.Y. Hein, C.A. Luber, I. Paron, N. Nagaraj, M. Mann, Mol. Cell. Proteomics 13 (2014) 2513–2526.
[36] M. Spinazzi, A. Casarin, V. Pertegato, L. Salviati, C. Angelini, Nat. Protoc. 7 (2012) 1235–1246.

[37] Kirby DM, Thorburn DR, Turnbull DM, Taylor RW. 2007;80:93–119.
[38] J. Park, Q. Tran, K. Mun, K. Masuda, S.H. Kwon, S.H. Kim, D.H. Kim, G. Thomas, J. Park, Cell. Signal. 28 (12) (Dec 2016) 1904–1915.
[39] L.S. Carnevalli, K. Masuda, F. Frigerio, O. Le Bacquer, S.H. Um, V. Gandin, I. Topisirovic, N. Sonenberg, G. Thomas, S.C. Kozma, Dev. Cell 18 (2010) 763–774.
[40] N. Ishihara, A. Jofuku, Y. Eura, K. Mihara, Biochem. Biophys. Res. Commun. 301 (2003) 891–898.
[41] G. Twig, A. Elorza, A.J. Molina, H. Mohamed, J.D. Wikstrom, G. Walzer, L. Stiles, S.E. Haigh, S. Katz, G. Las, J. Alroy, M. Wu, B.F. Py, J. Yuan, J.T. Deeney, B.E. Corkey, O.S. Shirihai, EMBO J. 27 (2008) 433–446.
[42] D.R. Green, L. Galluzzi, G. Kroemer, Science 345 (2014) 1250256.
[43] L. Galluzzi, O. Kepp, G. Kroemer, Microb. Cell 3 (2016) 101–108.
[44] C. Lopez-Otin, L. Galluzzi, J.M. Freije, F. Madeo, G. Kroemer, Cell 166 (2016) 802–821.
[45] M.R. Tavares, I.C. Pavan, C.L. Amaral, L. Meneguello, A.D. Luchessi, F.M. Simabuco, Life Sci. 131 (2015) 1–10.
[46] B. Magnuson, B. Ekim, D.C. Fingar, Biochem. J. 441 (2012) 1–21.
[47] I.A. Stanley, S.M. Ribeiro, A. Gimenez-Cassina, E. Norberg, N.N. Danial, Trends Cell Biol. 24 (2014) 118–127.
[48] A.J. Molina, J.D. Wikstrom, L. Stiles, G. Las, H. Mohamed, A. Elorza, G. Walzer, G. Twig, S. Katz, B.E. Corkey, O.S. Shirihai, Diabetes 58 (2009) 2303–2315.
[49] B. Kruspig, A. Nilchian, I. Bejarano, S. Orrenius, B. Zhivotovsky, V. Gogvadze, Cell. Mol. Life Sci. 69 (2012) 2091–2099.
[50] S. Orrenius, V. Gogvadze, B. Zhivotovsky, Biochem. Biophys. Res. Commun. 460 (2015) 72–81.
[51] A.S. Rambold, B. Kostelecky, N. Elia, J. Lippincott-Schwartz, Proc. Natl. Acad. Sci. U. S. A. 108 (2011) 10190–10195.
[52] L.C. Gomes, G. Di Benedetto, L. Scorrano, Nat. Cell Biol. 13 (2011) 589–598.
[53] E.B. Arias, J. Kim, K. Funai, G.D. Cartee, Am. J. Physiol. Endocrinol. Metab. 292 (2007) E1191–1200.
[54] J. Jensen, P.I. Rustad, A.J. Kolnes, Y.C. Lai, Front. Physiol. 2 (2011) 112.